Direct observation of spin accumulation in Cu induced by spin pumping

Junjia Ding,[1,*] Wei Zhang,[2,1] M. Benjamin Jungfleisch,[3,1] John E. Pearson,[1]
Hendrik Ohldag,[4,5,6] Valentine Novosad,[1] and Axel Hoffmann[1,7,†]

[1]*Materials Science Division, Argonne National Laboratory, Argonne, Illinois 60439, USA*
[2]*Department of Physics, Oakland University, Rochester, Michigan 48309, USA*
[3]*Department of Physics and Astronomy, University of Delaware, Newark, Delaware 19716, USA*
[4]*Stanford Synchrotron Radiation Laboratory, SLAC National Accelerator Laboratory, 2575 Sand Hill Road, Menlo Park, California 94025, USA*
[5]*Advanced Light Source, Lawrence Berkeley National Laboratory, Berkeley, California 94710, USA*
[6]*Department of Physics, University of California Santa Cruz, Santa Cruz, California 95064, USA*
[7]*Department of Materials Science and Engineering, University of Illinois at Urbana-Champaign, Urbana, Illinois 61801, USA*

(Received 7 June 2019; revised manuscript received 26 November 2019; accepted 10 January 2020; published 5 March 2020)

Pure spin currents have been ubiquitous in contemporary spintronics research. Despite its profound physical and technological significance, the detection of pure spin current has largely remained indirect, which is usually achieved by probing spin-transfer torque effects or spin-to-charge conversions. By using scanning transmission x-ray microscopy, we report the direct detection and spatial mapping of spin accumulation in a nonmagnetic Cu layer without any direct charge current injection. Such a pure spin current is induced by spin pumping from a $Ni_{80}Fe_{20}$ layer and is not accompanied by concomitant charge motion. The observed frequency dependence indicates that the signal is dominated by a coherent, pure spin current, but the magnitude of the spin accumulation suggests also possible additional thermal contributions. Our technique takes advantage of the x-ray magnetic circular dichroism and the synchronization of microwave with x-ray pulses, which together provide a high sensitivity for probing transient magnetic moment. From the detected x-ray signals, we observe two distinct resonance modes induced by spin pumping, which, based on micromagnetic simulations, we attribute to nonlinear microwave excitations. Our result provides a new pathway for detecting pure spin currents that originate from many spintronics phenomena, such as spin Hall and spin Seebeck effects, and which can be applied to both metal and insulator spin current sources.

DOI: 10.1103/PhysRevResearch.2.013262

I. INTRODUCTION

Spin currents have been regarded as key ingredients for future energy-efficient electronic devices [1]. Conventionally, spin currents can be generated by passing an initially unpolarized charge current through a metallic ferromagnet, for example, in a spin-valve structure [2] or magnetic tunnel junction [3,4]. The charge flow then carries a net spin polarization and is known as a spin-polarized current. Furthermore, mechanisms relying on spin-orbit coupling, such as spin Hall effects [5,6], or magnon excitations, such as spin pumping [7,8] and spin Seebeck effect [9], allow the decoupling of the charge and spin currents and therefore, the generation of a "pure spin current," via charge currents, microwave excitations, or thermal gradients. In particular, the spin-pumping mechanism generates coherent spin current from magnetization dynamics, which offers unique opportunities for the synchronization with other dynamical physics parameters in the GHz frequency range. The generation and detection of the spin current are important technical aspects for making such a concept truly convincing. To date, on the detection side, the spin current is mostly indirectly detected, from either the spin-to-charge conversion [7,8,10–13], or its microscopic exchange interaction, known as the spin-transfer torque [14], with an adjacent magnetization. The resultant magnetization effects, such as tilting [15], switching [16], and excitation [17], are then probed either electrically [18–20] or optically [21–24], to elucidate the existence of spin current and its properties. For example, one can use the spin Hall effect of heavy metals to generate spin-orbit torques and drive the magnetization precession of an adjacent ferromagnet, known as the spin-torque ferromagnetic resonance (ST-FMR) [17], and then probe the ferromagnetic resonance (FMR) by electrical and optical means. In particular, the ferromagnet can be both metallic [17,19,20,22], or insulating [21,23,25,26] in this case owing to the decoupled charge current and pure spin current, which may offer additional advantages for energy efficiency.

While indirect measurements can provide useful insights, it is also important to explore techniques that enable direct

*Present address: Verily Life Sciences LLC, South San Francisco, CA.
†axelh@illinois.edu

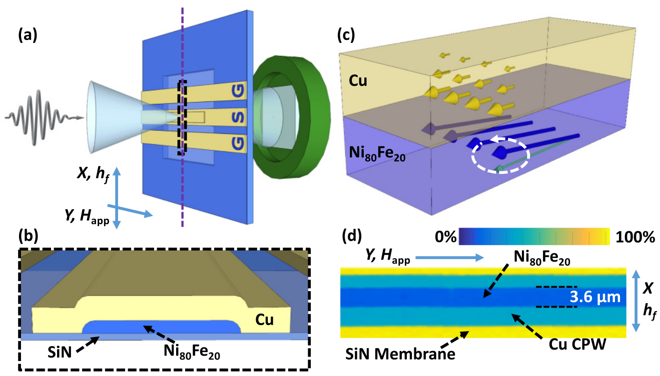

FIG. 1. (a) Schematic of the experiment setup using the STXM at the SSRL. An x-ray beam is focused onto the $Cu/Ni_{80}Fe_{20}/Si_3N_4$ structure. Microwave radio frequency current is delivered to the sample via the Cu CPW. (b) Cross-section of the film structure. (c) Schematic of spin pumping. Spin current is generated from the magnetization dynamics of $Ni_{80}Fe_{20}$ and then injected into the Cu layer. (d) X-ray transmission image of the CPW signal-line and central $Ni_{80}Fe_{20}$ stripe.

detection of spin current and spin accumulation. Although optical detection through magneto-optic Kerr effect is possible [27], the effect is very small and thus spatial imaging becomes very difficult and is limited by the optical diffraction limit to at best μm length scales. To overcome these limitations, one of the most promising techniques is to use highly-sensitive x-ray microscopy and spectroscopy, which can measure extremely small, transient x-ray magnetic circular dichroism (XMCD) effect from electronic spins [28]. Although direct detection of spin accumulations using XMCD is challenging [29], it has been directly observed that the spin accumulation in Cu induced by a spin-polarized current accounts for a transient magnetic moment of $\sim 10^{-5} \mu_B$ [30]. However, direct observation of the pure spin current-induced spin accumulation is still sparse [31], and a direct spatial mapping of such spin accumulation in a nonmagnetic material remains missing.

In this work, we report a direct experimental detection of spin-pumping-induced spin accumulation in Cu in $Ni_{80}Fe_{20}/Cu$ thin-film bilayers at room temperature, using the scanning transmission x-ray microscopy (STXM) at the Stanford Synchrotron Radiation Light-source (SSRL). Note that spin-pumping-induced spin accumulation from $Ni_{80}Fe_{20}$ into Cu has already been demonstrated [32]. The device structure consists of a microstructured $Ni_{80}Fe_{20}$ stripe fabricated on top of a Si_3N_4 membrane window and then capped with a Cu coplanar waveguide (CPW). Using a broadband ferromagnetic resonance technique, we systematically investigated the STXM spectra under GHz microwave excitations. We found a clear change in the STXM spectra at the Cu absorption edge as a function of the excitation frequency. Our experiment allowed a direct spatial mapping of the spin accumulation at the $Ni_{80}Fe_{20}/Cu$ interface induced by the spin pumping.

II. EXPERIMENTAL SETUP

Figure 1(a) is the schematics of our measurement setup. Circularly polarized x-rays generated at Beamline 13 at SSRL are focused onto the sample with a beam diameter $\sim$100 nm. The focused x-rays go through the $Cu/Ni_{80}Fe_{20}$ multilayer thin-film structure and the Si_3N_4 membrane, shown in Fig. 1(b), and then to an x-ray detector. The samples were fabricated on commercially available Si_3N_4 membrane windows (0.25 mm $\times$ 0.25 mm $\times$ 100 nm) on Si substrates. On each device, a $Ni_{80}Fe_{20}$ stripe (3.6 μm $\times$ 100 μm $\times$ 40 nm) was prepared at the center of the Si_3N_4 membrane window using photolithography followed by sputter deposition and lift-off process. A ground-signal-ground (G-S-G) type CPW made of Cu(70 nm)/Al(5 nm) was then sputter-deposited on top of the sample with the central signal-line covering the entire $Ni_{80}Fe_{20}$ stripe. The Cu layer has a dual-role: it serves as the spin current drain for the XMCD observation (tuned to Cu L_3-edge), and also excites the FMR of the $Ni_{80}Fe_{20}$ stripe. The microwave excitation was fixed at 20 dBm for maximized signals.

Upon FMR excitation, a pure spin current is generated at the $Cu/Ni_{80}Fe_{20}$ interface due to the spin-pumping effect and induces a transient spin accumulation in Cu, as is illustrated in Fig. 1(c). Such a finite spin accumulation can be sensitively probed by the XMCD effect using the STXM setup. For elemental specificity and optimal sensitivity, we tune the x-ray energy to the L_3-edge of Cu (935.197 eV). Figure 1(d) shows the x-ray transmission intensity of the sample. In addition, an external magnetic field (H_{app}) is applied along the stripe (along the y axis). Since the XMCD probes the component of the Cu magnetization along the incident direction of the x-rays, we also tilt the sample plane 45° with respect to the dashed line in Fig. 1(a).

Before imaging the sample using STXM we characterized the ferromagnetic resonance using a vector network analyzer and an radio frequency (rf) power of 0 dBm, as shown in Fig. 2(a). The experimental results (dots) are fitted well by the Kittel formula (line), which yields a saturation magnetization $M_s = 815$ kA/m. Based on these measurements, we fixed the external field $H_{app} = 150$ Oe during the subsequent STXM measurements, which corresponds to a resonance frequency $\sim$4.8 GHz. We verified similar FMR signals simultaneously with the STXM measurements, using separate rf circuits and a microwave diode. The STXM experiment was carried out by synchronizing the microwave excitation (at 20 dBm) with the x-ray detection and SSRL's master clock. At each scanning position of the sample, the microwave excitation was switched on for the even ring-cycles (780 ns) and turned off for the odd ring cycles (780 ns). All data were recorded for a dwell time of 2500 ms.

III. XMCD IMAGING RESULTS

Figure 2(b) shows the x-ray transmission image of the scanned area covering the $Ni_{80}Fe_{20}$ stripe at off-resonance, which serves as a reference for the subsequent XMCD images. The darker region at the center of the image corresponds to the $Ni_{80}Fe_{20}$ stripe and it indicates that the x-rays were partially absorbed by the $Ni_{80}Fe_{20}$. By taking the averaged intensity along the y coordinate, we can plot the x-ray transmission profile, at and near the $Ni_{80}Fe_{20}$ stripe, as shown in Fig. 2(f). The STXM experiment was carried out systematically for different excitation frequencies in the range of 3.5 to 6.0 GHz.

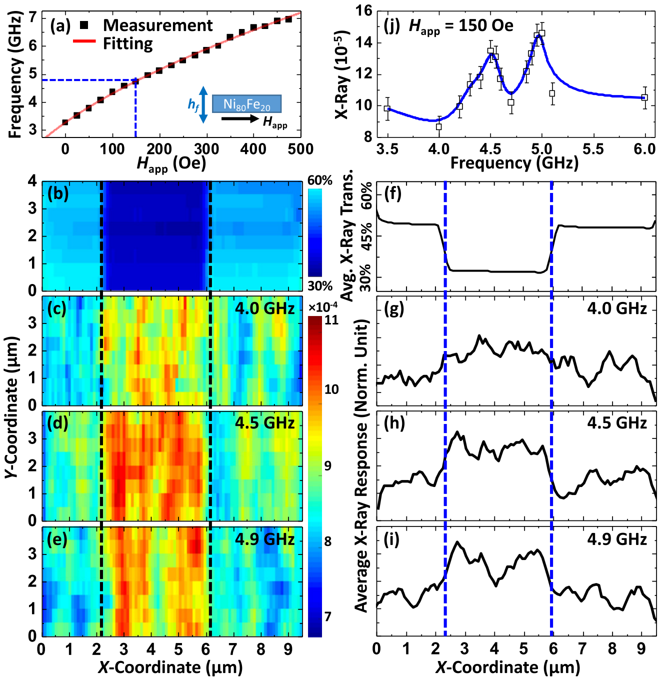

FIG. 2. (a) FMR measurement of the device and its Kittel relationship. (b) X-ray transmission image of an area covering the CPW signal-line. (c)–(e) STXM images of the same area at selective microwave excitation frequencies. The magnetic field is kept constant at 150 Oe. (f)–(i) Corresponding averaged signals along the y coordinate for panels (c)–(e). (j) Calculated x-ray contrast as a function of frequency.

For example, Figs. 2(c)–2(e) are the STXM contrast images at the same area but for selective excitation frequencies, $f = 4.0$, 4.5, and 4.9 GHz, respectively. The images were obtained by calculating the ratio of the x-ray transmission signal with the microwave excitation turned on and off. No clear spin accumulations were observed for $f = 4.0$ GHz, which is 0.8 GHz away from the FMR condition according to the dispersion in Fig. 2(a). However, a uniform excitation contrast was observed at the stripe area for $f = 4.5$ GHz, indicating spin accumulations in Cu induced by the spin-pumping effect. Further, at $f = 4.9$ GHz, interestingly, the edge of stripe exhibits a stronger signal than the center of the stripe, indicating possibly a stronger spin-pumping effect from the $Ni_{80}Fe_{20}$ edges. Such an effect can be observed clearly from the corresponding averaged intensity curves, shown in Figs. 2(g)–2(i). Here, the observed frequency dependence of the spin accumulation is also a strong indication of a coherent, pure spin current. The strength of the spin-pumping effect can be then evaluated by calculating the x-ray contrasts: $I = lg(I_s/I_{Cu})$, in which I_s is the averaged intensity in Cu at the stripe area and I_{Cu} is the intensity in the area that contains only Cu. The results at different frequencies are summarized in Fig. 2(j), exhibiting clearly a resonance profile with two maxima, which differs from the single excitation peak observed for the vector network analyzer based measurements; see Fig. 2(a). This suggests that the microwave power used during the XMCD experiment, i.e., 20 dBm, is likely already above the linear threshold for FMR spin pumping. Unfortunately, at lower microwave excitation power, the XMCD signal are too weak for a meaningful exploration of the power-dependence of these signals.

IV. THEORETICAL MODELING AND DISCUSSION

The dynamic magnetization profiles due to geometric confinement in soft magnetic materials have been studied extensively [33–37]. In particular, higher-order modes due to quantization along the stripe width have been commonly observed [38–40]. We note that the frequencies of these higher order modes are expected to be above the maximum frequency of 6 GHz in our experiments, indicating that the observed inhomogeneity is expected to be of different origin. To further understand the observed results, we performed micromagnetic simulations using the Mumax3 code [41].

Standard parameters for $Ni_{80}Fe_{20}$ are used, i.e., a gyromagnetic ratio 2.8 GHz/kOe, saturation magnetization, $M_s = 815$ kA/m, exchange constant, $A = 13 \times 10^{-12}$ J/m, damping constant 0.008, and an anisotropy constant $K_U = 0$. The cell size was fixed at $5 \times 5 \times 5$ nm^3. In particular, we performed the simulation at different microwave excitation powers to elucidate also any nonlinear effects. In our simulation, an AC magnetic field with an amplitude of $h_f = 20$ Oe is applied along the width of the stripe to simulate the microwave excitation from the G-S-G waveguide. We note that at such high microwave fields, nonlinear phenomena, such as Suhl instabilities, are readily observed [42,43]. The averaged response of the stripe for each frequency is summarized in Fig. 3(a). Two peaks can be observed at 4.5 and 4.9 GHz, which is in agreement with our experimental results. Figure 3(b) is a cross-section view of the intensity map at the stripe area as a function of the frequency. A uniform excitation can be observed at 4.5 GHz. However, the edge response is also quite pronounced, and extends to a much wider frequency range. These observations agree well with our experimental results summarized in Fig. 2. As a comparison, a set of similar simulation was performed with a much lower excitation power ($h_f = 1$ Oe). The simulation results show only one resonance mode around 4.7 GHz, as shown in Fig. 3(c), and the two-dimensional resonance map also suggests a nearly uniform excitation around 4.7 GHz.

Now that we see that the observed spatial profiles of the observed spin accumulation in Cu agree well with the frequency dependence of the expected spatial distribution of the magnetization dynamics, we will analyze also the signal magnitude quantitatively. Following the discussion in Ref. [30], we can estimate the induced magnetic moment per Cu atom from the XMCD contrast in Fig. 2(j). Taking into account the Cu thickness of 70 nm in our measurement, which is 2.5 times larger than in the earlier experiment [30], we can estimate a magnetization of $2 \times 10^{-4}\ \mu_B$ per Cu atom. At the same time the spin current from spin pumping is given by [8]

$$j_s = \frac{\hbar\omega}{4\pi}\mathrm{Re}(2g_{\uparrow\downarrow})\sin^2(\theta), \tag{1}$$

where ω is the resonance frequency, $g_{\uparrow\downarrow}$ is the spin-mixing conductance, and θ is the precession cone angle of the FMR. From earlier measurements on similar devices [44], we can

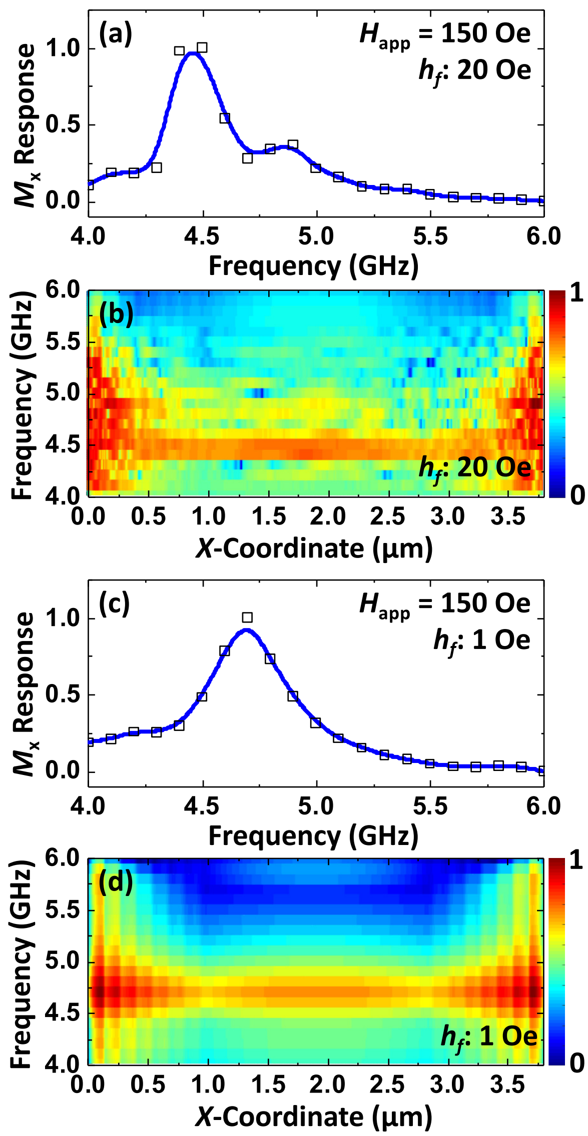

FIG. 3. (a), (c) Simulated dynamical response of the $Ni_{80}Fe_{20}$ stripe at $h_f = 20$ Oe, and $h_f = 1$ Oe, respectively. (b), (d) The corresponding two-dimensional cross-section images of the resonance response in the area of interest.

estimate for our excitation power the precession cone angle to be about $\theta = 10^\circ$. Based on the nominal charge density of copper we can also estimate $g_{\uparrow\downarrow} = 1.5 \times 10^{19} \mathrm{m}^{-2}$, which is consistent with the values for most normal metals. We can now compare the injected spin-current in our experiment to earlier measurements with electrical injection [30], by converting the spin current into an equivalent charge current $j_c = (2e/\hbar) j_s = 3.3 \times 10^8 \mathrm{A/m^2}$. We note that this current density is about two orders of magnitude smaller (taken into account the finite spin polarization for the electrical injection), even though we estimate an injected moment from the spin pumping comparable to the previous measurement. This suggests that to explain our experimentally observed magnitude of spin accumulation, processes beyond spin pumping, such as thermal spin injection may be important. Given the high excitation power of 20 dBm, significant resonant heating of the permalloy stripe upon resonant excitation is possible [45]. However, a precise estimate of the temperature increase is difficult, and given the uncertainties of the spin Seebeck efficiency in all-metallic structure, a quantitative comparison is not straight forward.

V. CONCLUSIONS

In summary, by using scanning transmission x-ray microscopy measurements with x-ray circular dichroism (XMCD) contrast, we have observed spin accumulations in Cu induced by the spin-pumping effect. The observed spin accumulation depends on both the driving frequency and microwave power. Upon a strong microwave excitation, the XMCD effect at the Cu L_3 absorption edge indicates clearly a nonlinear resonance profile with dual-modes across the ferromagnet stripe. Specifically, the low-frequency mode is uniformly distributed across the stripe, while the high-frequency mode is primarily located at the edges of the stripe. The experimental results are further validated by using micromagnetic simulations. Our work provides direct evidence of the spin accumulation caused by a pure spin current that is not accompanied by any charge motion. Therefore, spatially resolved XMCD imaging may provide further detailed insights into the formation of spin accumulations from a wide variety of phenomena.

ACKNOWLEDGMENTS

Work at Argonne, including experimental design and measurement, sample fabrication, data analysis, and manuscript preparation, was supported by the US Department of Energy (DOE), Office of Science, Basic Energy Sciences, Materials Science and Engineering Division under Contract No. DE-AC02-06CH11357. Use of the Stanford Synchrotron Radiation Lightsource, SLAC National Accelerator Laboratory, is supported by the US Department of Energy, Office of Science, Office of Basic Energy Sciences under Contract No. DE-AC02-76SF00515. W.Z. acknowledges the DOE visiting Faculty Program.

[1] A. Hoffmann and S. D. Bader, Phys. Rev. Appl. **4**, 047001 (2015).
[2] B. Dieny, J. Magn. Magn. Mater. **136**, 335 (1994).
[3] T. Miyazaki and N. Tezuka, J. Magn. Magn. Mater. **139**, L231 (1995).
[4] J. S. Moodera, L. R. Kinder, T. M. Wong, and R. Meservey, Phys. Rev. Lett. **74**, 3273 (1995).
[5] J. Sinova, S. O. Valenzuela, J. Wunderlich, C. H. Back, and T. Jungwirth, Rev. Mod. Phys. **87**, 1213 (2015).
[6] A. Hoffmann, IEEE Trans. Magn. **49**, 5172 (2013).

[7] E. Saitoh, M. Ueda, H. Miyajima, and G. Tatara, Appl. Phys. Lett. **88**, 182509 (2006).
[8] O. Mosendz, J. E. Pearson, F. Y. Fradin, G. E. W. Bauer, S. D. Bader, and A. Hoffmann, Phys. Rev. Lett. **104**, 046601 (2010).
[9] K. Uchida, S. Takahashi, K. Harii, J. Ieda, W. Koshibae, K. Ando, S. Maekawa, and E. Saitoh, Nature **455**, 778 (2008).
[10] K. Ando, S. Takahashi, J. Ieda, Y. Kajiwara, H. Nakayama, T. Yoshino, K. Harii, Y. Fujikawa, M. Matsuo, S. Maekawa, and E. Saitoh, J. Appl. Phys. **109**, 103913 (2011).
[11] W. Zhang, M. B. Jungfleisch, W. Jiang, J. E. Pearson, A. Hoffmann, F. Freimuth, and Y. Mokrousov, Phys. Rev. Lett. **113**, 196602 (2014).
[12] W. Zhang, M. B. Jungfleisch, W. Jiang, J. Sklenar, F. Y. Fradin, J. E. Pearson, J. B. Ketterson, and A. Hoffmann, J. Appl. Phys. **117**, 172610 (2015).
[13] J. C. Rojas Sánchez, L. Vila, G. Desfonds, S. Gambarelli, J. P. Attané, J. M. De Teresa, C. Magén, and A. Fert, Nature Commun. **4**, 2944 (2013).
[14] D. C. Ralph and M. D. Stiles, J. Magn. Magn. Mater. **320**, 1190 (2008).
[15] S. Emori, U. Bauer, S. M. Ahn, E. Martinez, and G. S. D. Beach, Nature Mater. **12**, 611 (2013).
[16] L. Liu, C.-F. Pai, Y. Li, H. W. Tseng, D. C. Ralph, and R. A. Buhrman, Science **336**, 555 (2012).
[17] L. Liu, T. Moriyama, D. C. Ralph, and R. A. Buhrman, Phys. Rev. Lett. **106**, 036601 (2011).
[18] J. Sklenar, W. Zhang, M. B. Jungfleisch, H. Saglam, S. Grudichak, W. Jiang, J. E. Pearson, J. B. Ketterson, and A. Hoffmann, Phys. Rev. B **95**, 224431 (2017).
[19] W. Zhang, M. B. Jungfleisch, F. Freimuth, W. Jiang, J. Sklenar, J. E. Pearson, J. B. Ketterson, Y. Mokrousov, and A. Hoffmann, Phys. Rev. B **92**, 144405 (2015).
[20] T. Nan, S. Emori, C. T. Boone, X. Wang, T. M. Oxholm, J. G. Jones, B. M. Howe, G. J. Brown, and N. X. Sun, Phys. Rev. B **91**, 214416 (2015).
[21] M. B. Jungfleisch, W. Zhang, J. Sklenar, J. Ding, W. Jiang, H. Chang, F. Y. Fradin, J. E. Pearson, J. B. Ketterson, V. Novosad, M. Wu, and A. Hoffmann, Phys. Rev. Lett. **116**, 057601 (2016).
[22] X. Fan, H. Celik, J. Wu, C. Ni, K.-J. Lee, V. O. Lorenz, and J. Q. Xiao, Nature Commun. **5**, 3042 (2014).
[23] M. Montazeri, P. Upadhyaya, M. C. Onbasli, G. Yu, K. L. Wong, M. Lang, Y. Fan, X. Li, P. K. Amiri, R. N. Schwartz, C. A. Ross, and K. L. Wang, Nature Commun. **6**, 8958 (2015).
[24] Y. Li, H. Saglam, Z. Zhang, R. Bidthanapally, Y. Xiong, J. E. Pearson, V. Novosad, H. Qu, G. Srinivasan, A. Hoffmann, and W. Zhang, Phys. Rev. Appl. **11**, 034047 (2019).
[25] J. Sklenar, W. Zhang, M. B. Jungfleisch, W. Jiang, H. Chang, J. E. Pearson, M. Wu, J. B. Ketterson, and A. Hoffmann, Phys. Rev. B **92**, 174406 (2015).
[26] M. B. Jungfleisch, J. Ding, W. Zhang, W. Jiang, J. E. Pearson, V. Novosad, and A. Hoffmann, Nano Lett. **17**, 8 (2016).
[27] C. Stamm, C. Murer, M. Berritta, J. Feng, M. Gabureac, P. M. Oppeneer, and P. Gambardella, Phys. Rev. Lett. **119**, 087203 (2017).
[28] J. Stöhr, J. Magn. Magn. Mater. **200**, 470 (1999).
[29] O. Mosendz, G. Mihajlović, J. E. Pearson, P. Fischer, M.-Y. Im, S. D. Bader, and A. Hoffmann, Phys. Rev. B **80**, 104439 (2009).
[30] R. Kukreja, S. Bonetti, Z. Chen, D. Backes, Y. Acremann, J. A. Katine, A. D. Kent, H. A. Dürr, H. Ohldag, and J. Stöhr, Phys. Rev. Lett. **115**, 096601 (2015).
[31] J. Li, L. R. Shelford, P. Shafer, A. Tan, J. X. Deng, P. S. Keatley, C. Hwang, E. Arenholz, G. van der Laan, R. J. Hicken, and Z. Q. Qiu, Phys. Rev. Lett. **117**, 076602 (2016).
[32] T. Yamamoto, T. Seki, S. Ono, and K. Takanshi, J. Appl. Phys. **115**, 17C505 (2014).
[33] Y. Au, T. Davison, E. Ahmad, P. S. Keatley, R. J. Hicken, and V. V. Kruglyak, Appl. Phys. Lett. **98**, 122506 (2011).
[34] S. Tacchi, G. Duerr, J. W. Klos, M. Madami, S. Neusser, G. Gubbiotti, G. Carlotti, M. Krawczyk, and D. Grundler, Phys. Rev. Lett. **109**, 137202 (2012).
[35] T. Schwarze and D. Grundler, Appl. Phys. Lett. **102**, 222412 (2013).
[36] M. Krawczyk and D. Grundler, J. Phys.: Conden. Matter **26**, 123202 (2014).
[37] F. B. Mushenok, R. Dost, C. S. Davies, D. A. Allwood, B. J. Inkson, G. Krkac, and V. V. Kruglyak, Appl. Phys. Lett. **111**, 042404 (2017).
[38] C. Mathieu, J. Jorzick, A. Frank, S. O. Demokritov, A. N. Slavin, B. Hillebrands, B. Bartenlian, C. Chappert, D. Decanini, F. Rousseaux, and E. Cambril, Phys. Rev. Lett. **81**, 3968 (1998).
[39] J. Jorzick, S. O. Demokritov, C. Mathieu, B. Hillebrands, B. Bartenlian, C. Chappert, F. Rousseaux, and A. N. Slavin, Phys. Rev. B **60**, 15194 (1999).
[40] G. Gubbiotti, O. Kazakova, G. Carlotti, M. Hanson, and P. Vavassori, IEEE Trans. Magn. **39**, 2750 (2003).
[41] A. Vansteenkiste, J. Leliaert, M. Dvornik, M. Helsen, F. Garcia-Sanchez, and B. Van Waeyenberge, AIP Adv. **4**, 107133 (2014).
[42] H. M. Olson, P. Krivosik, K. Srinivasan, and C. Paton, J. Appl. Phys. **102**, 023904 (2007).
[43] H. G. Bauer, P. Majchrak, T. Kachel, C. H. Back, and G. Woltersdorf, Nature Commun. **6**, 8274 (2015).
[44] V. Vlaminck, J. E. Pearson, S. D. Bader, and A. Hoffmann, Phys. Rev. B **88**, 064414 (2013).
[45] H. Schultheiss, J. E. Pearson, S. D. Bader, and A. Hoffmann, Phys. Rev. Lett. **109**, 237204 (2012).